


Data Quality and Optimal Background Correction Order of Respiratory-Gated *k*-Space Segmented Spoiled Gradient Echo (SGRE) and Echo Planar Imaging (EPI)-Based 4D Flow MRI

Federica Viola, MSc,^{1*}  Petter Dyverfeldt, PhD,^{1,2} Carl-Johan Carlhäll, MD, PhD,^{1,2,3} and Tino Ebbers, PhD^{1,2}

Background: A reduction in scan time of 4D Flow MRI would facilitate clinical application. A recent study indicates that echo-planar imaging (EPI) 4D Flow MRI allows for a reduction in scan time and better data quality than the recommended *k*-space segmented spoiled gradient echo (SGRE) sequence. It was argued that the poor data quality of SGRE was related to the nonrecommended absence of respiratory motion compensation. However, data quality can also be affected by the background offset compensation.

Purpose: To compare the data quality of respiratory motion-compensated SGRE and EPI 4D Flow MRI and their dependence on background correction (BC) order.

Study Type: Retrospective.

Subjects: Eighteen healthy subjects (eight female, mean age 32 ± 5 years).

Field Strength and Sequence: 1.5 T. [Correction added on July 26, 2019, after first online publication: The preceding field strength was corrected.] SGRE and EPI-based 4D Flow MRI.

Assessment: Data quality was investigated visually and by comparing flows through the cardiac valves and aorta. Measurements were obtained from transvalvular flow and pathline analysis.

Statistical Tests: Linear regression and Bland–Altman analysis were used. Wilcoxon test was used for comparison of visual scoring. Student's *t*-test was used for comparison of flow volumes.

Results: No significant difference was found by visual inspection ($P = 0.08$). Left ventricular (LV) flows were strongly and very strongly associated with SGRE and EPI, respectively ($R^2 = 0.86$ – 0.94 SGRE; 0.71 – 0.79 EPI, BC0–4). LV and right ventricular (RV) outflows and LV pathline flows were very strongly associated ($R^2 = 0.93$ – 0.95 SGRE; 0.88 – 0.91 EPI, $R^2 = 0.91$ – 0.95 SGRE; 0.91 – 0.93 EPI, BC1–4). EPI LV outflow was lower than the short-axis-based stroke volume. EPI RV outflow and proximal descending aortic flow were lower than SGREs.

Data Conclusion: Both sequences yielded good internal data consistency when an adequate background correction was applied. Second and first BC order were considered sufficient for transvalvular flow analysis in SGRE and EPI, respectively. Higher BC orders were preferred for particle tracing.

Level of Evidence: 4

Technical Efficacy Stage: 1

J. MAGN. RESON. IMAGING 2020;51:885–896.

View this article online at wileyonlinelibrary.com. DOI: 10.1002/jmri.26879

Received Feb 27, 2019, Accepted for publication Jul 10, 2019.

*Address reprint requests to: F.V., Linköping University, Division of Cardiovascular Medicine, Department of Medical and Health Sciences, SE-581 85 Linköping, Sweden. E-mail: federica.viola@liu.se

Contract grant sponsor: Swedish Research Council; Contract grant number: 621-2014-6191; Contract grant sponsor: Swedish Heart and Lung Foundation; Contract grant number: 20140398.

From the ¹Division of Cardiovascular Medicine, Department of Medical and Health Sciences, Linköping University, Linköping, Sweden; ²Center for Medical Image Science and Visualization (CMIV), Linköping University, Linköping, Sweden; and ³Department of Clinical Physiology, Department of Medical and Health Sciences, Linköping University, Linköping, Sweden

Additional supporting information may be found in the online version of this article

This is an open access article under the terms of the Creative Commons Attribution-NonCommercial License, which permits use, distribution and reproduction in any medium, provided the original work is properly cited and is not used for commercial purposes.

TIME-RESOLVED 3D PHASE-CONTRAST magnetic resonance imaging (4D Flow MRI) is increasingly used in research and clinical settings. As it allows for retrospective placement of analysis planes in the acquired volume, 4D Flow MRI lends itself well for flow visualization and flow volume quantification, including at locations in the cardiovascular system not easily reached with other modalities. Initial clinical applications include assessment of flow patterns and volumes in the setting of, eg, congenital heart disease, aortic disease, regurgitant heart valve disease, shunts, and collateral vessels.^{1–5}

Although 4D Flow MRI is on the verge to widespread clinical application, a few limitations still need to be addressed to facilitate implementation in clinical practice. Some of these challenges include reducing the scan time and optimizing the approach to reduce velocity quantification errors caused by eddy-current-induced background phase offsets.⁶

Several approaches to speed up data acquisition have been introduced, including fast sequences such as echo-planar imaging (EPI) and spiral imaging, as well as parallel imaging, k - t acceleration techniques, and compressed sensing strategies.^{7–18} However, all these strategies incur specific limitations and therefore a compromise between data quality and scan time must be reached. The 4D Flow consensus statement recommends a spoiled gradient sequence (SGRE) with parallel imaging factor two or three.⁶ A recent study compared an SGRE, an EPI, and a k - t BLAST-based sequence and concluded that the SGRE sequence produced lower data quality than the EPI sequence.¹⁹ The authors speculated that the unexpected better data quality of EPI was related to a reduction of motion-related artifacts due to the fast EPI k -space filling strategy and that the absence of respiratory motion compensation might have hampered the performance of the conventional 4D-SGRE sequence.¹⁹ As the type of sequence and approach to data undersampling affects the appearance of eddy-current-induced background phase offsets, the reduced data quality of the 4D-SGRE sequence might also be related to a suboptimal background offset correction. Furthermore, artifacts due to, for example, respiratory motion can complicate the in vivo background offset correction.⁶ Therefore, background phase offsets can often not be completely removed in vivo.^{20–23} A recent study recommends a first-order polynomial fit for background correction for in vivo datasets with static tissue below 60% of the total available volume, as higher orders may result in an overcorrection.²⁴ Conversely, a previous investigation showed that a first-order polynomial correction may be insufficient.²⁵

Hence, we set out to investigate and compare the data quality of respiratory motion-compensated SGRE and EPI-based 4D Flow MRI acquisitions and their dependence on background correction order.

Materials and Methods

The study was approved by Regional Ethical Board. All subjects gave informed consent to participate in the study. None of the authors had any competing interests in the study.

MR Scans and Processing

Eighteen healthy subjects (eight female, mean age 32 ± 5 years) underwent an MRI examination with a Philips 1.5T MRI system (Ingenua, Philips Healthcare, Best, The Netherlands). The scan protocol included balanced steady-state free-precession (bSSFP) images, acquired at end-expiratory breath-holds, and two free-breathing, respiratory-motion-compensated, 4D Flow examinations. The cine-bSSFP images consisted of a cardiac short-axis (SA) stack with in-plane spatial resolution of $1 \times 1 \text{ mm}^2$, slice thickness of 6 mm, and through-plane resolution of 6 mm, two-, and three-chamber long-axis images (2ch-, 3ch-images) of the left heart, a cardiac four-chamber long-axis image (4ch-image), and a 3ch-image of the right heart, with the same in-plane resolution as the SA stack.

Two retrospectively cardiac gated and respiratory navigator gated 4D Flow MRI examinations were performed; an EPI sequence with read-out factor 3 (three k -space lines were acquired within the same repetition time [TR] for every velocity encoding gradient) and a SGRE sequence with k -space segmentation factor 2 (a first k -space line was acquired for all four velocity-encoding gradients, followed by a second k -space line for all four velocity-encoding gradients, which was repeated over the cardiac cycle), as suggested in the 4D flow MRI consensus paper.⁶ The EPI read-out factor was set to 3 to obtain a similar acquired temporal resolution to SGRE. Temporal resolutions for EPI and SGRE were 30 msec and 40 msec, respectively.

Weighted navigator gating was used with a 5-mm window size in the inner 25% of k -space and 20 mm in outer k -space. Scan parameters included: a sagittal-oblique slab covering the whole heart and the thoracic aorta, velocity encoding range (VENC) 120 cm/s, flip angle 5° , acquired spatial resolution $2.9 \times 2.9 \times 2.9 \text{ mm}^3$. The 4D Flow images were reconstructed to 40 timeframes. The field of view (FOV) and the number of reconstructed slices was equal for the two 4D Flow acquisitions (matrix size [112, 112, 39–47]). Echo time (TE) and TR were 3 and 5 msec for SGRE, and 4 and 7 msec for EPI, respectively. Both sequences used parallel imaging SENSE factor 2 in the AP (anterior–posterior) and RL (right–left) phase-encoding direction. Typical scan times for SGRE and EPI were 10 and 8 minutes, respectively, navigator excluded. The average navigator gating efficiency was 60–80%. All 4D Flow data were corrected for concomitant gradient fields on the scanner, and corrected for phase wraps during postprocessing.²⁶

Background Phase Offsets

Correction for background phase offset was based on polynomial fitting of the velocity in static tissue.²⁵ The static tissue mask consisted of a *soft mask* (w), obtained by combining the magnitude image (m) with the temporal standard deviation of the velocity data:

$$w(x, y, z, t) = \frac{m(x, y, z, t)}{(SD(x, y, z))^p}$$

The coefficient p determines the weight given to the standard deviation, and was set to 2. Subsequently, the soft mask was used in a minimization problem to obtain the polynomial fit. The optimal choice of the polynomial order depends on several factors, including the spatial distribution of the offset and on the amount of static tissue present in the acquired volume; higher-order polynomial fitting would require many voxels containing static tissue spread out over the volume of interest. The use of a soft mask instead of a binary mask was designed to relax this constraint and consequently improve the robustness of the correction. In this study, five different fitted polynomial orders were tested, resulting in five different background corrections (BC): zero (BC0), first (BC1), second (BC2), third (BC3), and fourth order (BC4).

Visual Evaluation of Data Quality

Data quality of SGRE and EPI was blindly evaluated by three observers, (T.E., P.D., and F.V.), with 22, 14, and 5 years of experience, respectively, in 4D Flow MRI. The evaluation was based on the magnitude and phase images, previous background, and phase wrapping corrections, which were judged according to a 4-point-Likert scale and inspected for blurring artifacts (on both phase and magnitude images), phase wrapping (on phase images), respiratory motion artifact (on magnitude images), and signal void. Phase images were corrected with BC order 2 before the visual evaluation. The following grades were assigned to each dataset: A: excellent quality, no artifacts in the magnitude and phase images; B: good quality, some blurring or respiratory artifacts on the magnitude image, no artifact on phase; C: moderate quality, artifacts on both type of images; D: poor quality, severe artifacts.

Transvalvular Flow Volume Analysis

Transvalvular flow measurements were performed on all datasets, for each BC order, to inspect whether the volumetric blood flow entering and exiting the heart would match. The analysis was performed by retrospectively placing planes over the cardiac valve of interest, and computing volumetric stroke volumes, while accounting for valve motion.²⁷ In this way, left ventricular (LV) inflow, LV outflow, and right ventricular (RV) outflow were thus obtained, by automatically tracking the valve on the respective 3ch-image (left sided 3ch for the aortic and mitral valve and right sided 3ch for pulmonary valve). The valve tracking was used to assess both the SGRE and EPI data to assure the same valve planes. The tracking method used was based on the Kanade–Lucas–Tomasi algorithm.²⁸

Aortic Flow Volume Analysis

In addition to transvalvular flow analysis, flow volumes were computed at two locations in the aorta, just distal to the left subclavian artery in the proximal descending aorta, and in the distal descending aorta at the diaphragm level. The position of the analysis plane was fixed during the whole cardiac cycle.

Pathline Analysis

Pathline analysis was performed for all sequences for BC order 0 to 4, using previously described methods.²⁹ Based on the bSSFP SA stacks, the left ventricle was manually segmented at end-diastole and end-systole using the freely available software Segment v. 2.0 R5673 (<http://segment.heiberg.se>).³⁰ Pathlines were emitted at end-diastole

from the LV and followed backward and forward in time until end-systole. Subsequently, inflow (flow entering the left ventricle) and outflow (flow exiting the left ventricle) stroke volumes, and the "invalid" pathlines, were computed. The invalid pathlines, denoted as "nonphysiological flow," consist of the pathlines generated inside the LV at end-diastole that have exited the ventricle at end-systole without passing through the segmentation's most basal plane. Inflow and outflow volumes were compared to test their agreement, while nonphysiological flow, representing the flow exiting the cardiac cavity without following any physiological route, was assessed, as it is sensitive to background phase offsets in the data. Two datasets were excluded from this part of the analysis because of major spatial mismatch between 4D Flow data and SA-image, due to the movement of the subjects between the scans. Another dataset presented a minor spatial mismatch between 4D Flow data and SA-image, which required a manual alignment of the segmentation to the 4D Flow data.

SA-Based Stroke Volume

The SA segmentations were used to compute the LV stroke volume (LVSFV) by calculating the difference between the end-diastolic volume (EDV) and the end-systolic-volume (ESV).

Velocity Profile Analysis

Furthermore, the velocity profile at peak systole through a cross-section of the thoracic descending aorta was calculated, to detect possible peak velocity and velocity gradient differences between the two acquisitions. The plane location was 2 cm downstream of the plane used for flow assessment in the proximal descending aorta (see the "Aortic Flow Volume Analysis" section). After the velocity profile was obtained, the slope of the curve was calculated, by fitting a line between the pixel closest to the wall and a pixel at 2/3 of the highest velocity. Subsequently, a paired t -test was used to determine if the mean difference between the EPI and SGRE slopes were zero.

Statistical Analysis

Using the Kolmogorov–Smirnov test for skewness and the Shapiro–Wilk test for kurtosis, we could not prove that the data were not normally distributed. Linear regression analysis and Bland–Altman analysis were performed to test internal data consistency. In this study, a flow mean difference (mean_d) lower than 5% was considered the threshold to good quality.³¹ A Wilcoxon test was used for paired comparison of visual scoring of data quality. Student's t -test was used for paired comparison of flow volumes. The results were considered statistically different for a $P < 0.05$, with a level of significance $\alpha = 0.05$. Association, derived from the determination coefficients, was considered weak with $R^2 \leq 0.25$, moderate $0.25 < R^2 \leq 0.5$, strong $0.5 < R^2 \leq 0.8$, very strong $0.8 < R^2 \leq 1$.

Results

Visual Evaluation of Data Quality

Visual inspection of 4D Flow images (phase in three directions and magnitude) found no significant difference between EPI and SGRE ($P = 0.08$). Figure 1a shows an example of images for both sequences, from one dataset that exhibited phase wrapping (visible in the Phase RL images),

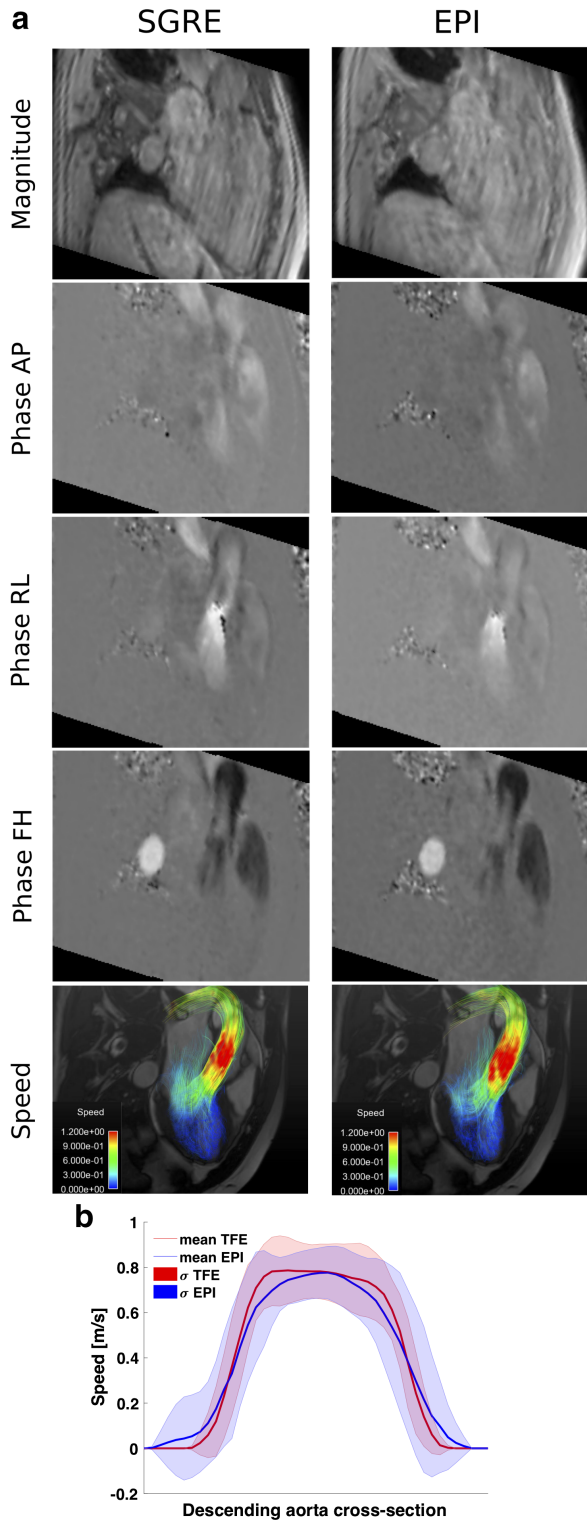


FIGURE 1: Comparison between SGRE and EPI data. **a:** Magnitude image, phase image acquired in the AP (anterior-posterior) direction, phase image in the RL (right-left) direction, phase image in the FH (feet-head) direction and streamlines plotted on a reference left sided 3ch-image. Streamlines do not show any visible abnormal velocity profile. **b:** Speed at peak systole through a cross-section of the thoracic descending aorta in SGRE (red) and EPI (blue) data. Mean values of all subjects are represented as solid lines, and standard deviation as shaded areas. Magnitude and phase images, streamlines, and velocity profiles shown were obtained with BC2.

subsequently corrected in postprocessing. Table 1 reports the cumulative scores from both observers. The interrater reliability (IRR) was 61%.

Transvalvular Flow Volume Analysis

LV inflow and outflow and RV and LV outflow for SGRE and EPI were compared at every BC order (Fig. 2a,b). Flow measurements for BC order 0 to 4 were very strongly associated for LV inflow and outflow in SGRE ($R^2 = 0.86, 0.90, 0.89, 0.91, 0.94$) and strongly associated in EPI ($R^2 = 0.71, 0.73, 0.76, 0.79, 0.76$). RV and LV outflow showed very strong associations, at every BC for both sequences ($R^2 = 0.85, 0.93, 0.95, 0.94, 0.95$ SGRE; $R^2 = 0.91, 0.91, 0.88, 0.88, 0.90$ EPI). The mean and standard deviation values of all the subjects at every BC are reported in Table 2. All EPI RV volume measurements were lower compared with the SGREs with BC applied (*P*-values reported in Table 3), while no difference was found between LV measurements, even if there is a trend of slightly smaller volumes for EPI.

The Bland-Altman analysis yielded a mean difference lower than 5% for LV inflow vs. outflow when using BC2-to-4 in SGRE and BC1-to-4 in EPI. For LV outflow vs. RV outflow, all the mean differences were smaller than 5%, with BC applied. The Bland-Altman analysis coefficients for every BC order are reported in Table 4. Paired Student’s *t*-test results between measurements at increasing BC, eg, BC0 LV inflow vs. BC1 LV inflow, are reported in Supplementary Table 1.

Aortic Flow Volume Analysis

Flow volume measurements at multiple locations in the aorta for SGRE and EPI are summarized in Fig. 3 and Table 2. For SGRE, the results showed a 33% mean flow decrease (mean for all BC) between the aortic valve and the proximal descending aorta, due to the blood flowing to the coronary arteries and the supra aortic arteries, and a 1.6% decrease between proximal and distal descending aorta. For EPI, at the proximal descending aorta the mean flow volume decreased by 35%, compared with the aortic valve plane, and a 1.4% decrease between proximal and distal descending aorta. Table 2 shows the flow volumes mean and standard deviation for SGRE and EPI data, at each BC order.

SGRE and EPI Association at Different Locations

We computed the association between SGRE and EPI measurements at each plane location, ie, the aortic valve (LV outflow), mitral valve (LV inflow), pulmonary valve (RV outflow), and proximal and distal descending aorta. SGRE and EPI LV outflows, RV outflows, and flow measurements at the distal descending aorta were very strongly associated ($R^2 = 0.82, 0.85, 0.80, 0.81, 0.82, R^2 = 0.87, 0.86, 0.88, 0.84, 0.90, R^2 = 0.78, 0.82, 0.83, 0.83, 0.83$) in increasing BC order respectively. SGRE and EPI LV inflows

TABLE 1. Visual Inspection Scores

SGRE	Scores			EPI	Scores		
	A	B	C		A	B	C
Ref 1	5	12	1	Ref 1	1	15	2
Ref 2	7	11	0	Ref 2	5	12	1
Ref 3	5	10	3	Ref 3	3	12	3
Total	17	33	4	Total	9	39	6

and flow measurements at the proximal descending aorta were moderately to very strongly associated ($R^2 = 0.71, 0.68, 0.83, 0.80, 0.79, R^2 = 0.46, 0.79, 0.75, 0.64, 0.77$) in increasing BC order, respectively (Fig. 1, Supplementary Material).

Pathline Analysis

LV inflow and outflow were strongly associated ($R^2 = 0.95, 0.97, 0.91, 0.93, 0.93$ SGRE; $R^2 = 0.98, 0.97, 0.92, 0.95, 0.98$ EPI) (Table 2 and Fig. 2c). No differences emerged

between EPI and SGRE measurements at all BC orders higher than one for the LV inflow, and higher than zero for the outflow.

The nonphysiological flow, expressed as mean \pm standard deviation, is shown Table 5. In EPI data, the nonphysiological flow decreased when stepping from BC1 to BC2 and from BC2 to BC3, while for SGRE measurements it decreased at each BC increment (Table 5). The nonphysiological flow was reduced by 52% and 32% in SGRE and EPI, respectively, when the BC order applied was at least three. No reduction was observed when using BC4 instead of BC3 for EPI. The nonphysiological flow was lower for EPI compared with SGRE, for all BC order, except for order 4, where there was no difference (Table 3).

LVSF

The LVSF was 92.0 ± 20.8 ml. LVSF and LV outflow of SGRE and EPI data were very strongly associated ($R^2 = 0.85, 0.86, 0.84, 0.84, 0.85$ SGRE; $R^2 = 0.96, 0.96, 0.94, 0.94, 0.95$ EPI, in increasing BC order) (Fig. 4). The slope value of the linear regression for EPI and SGRE were comparable, and

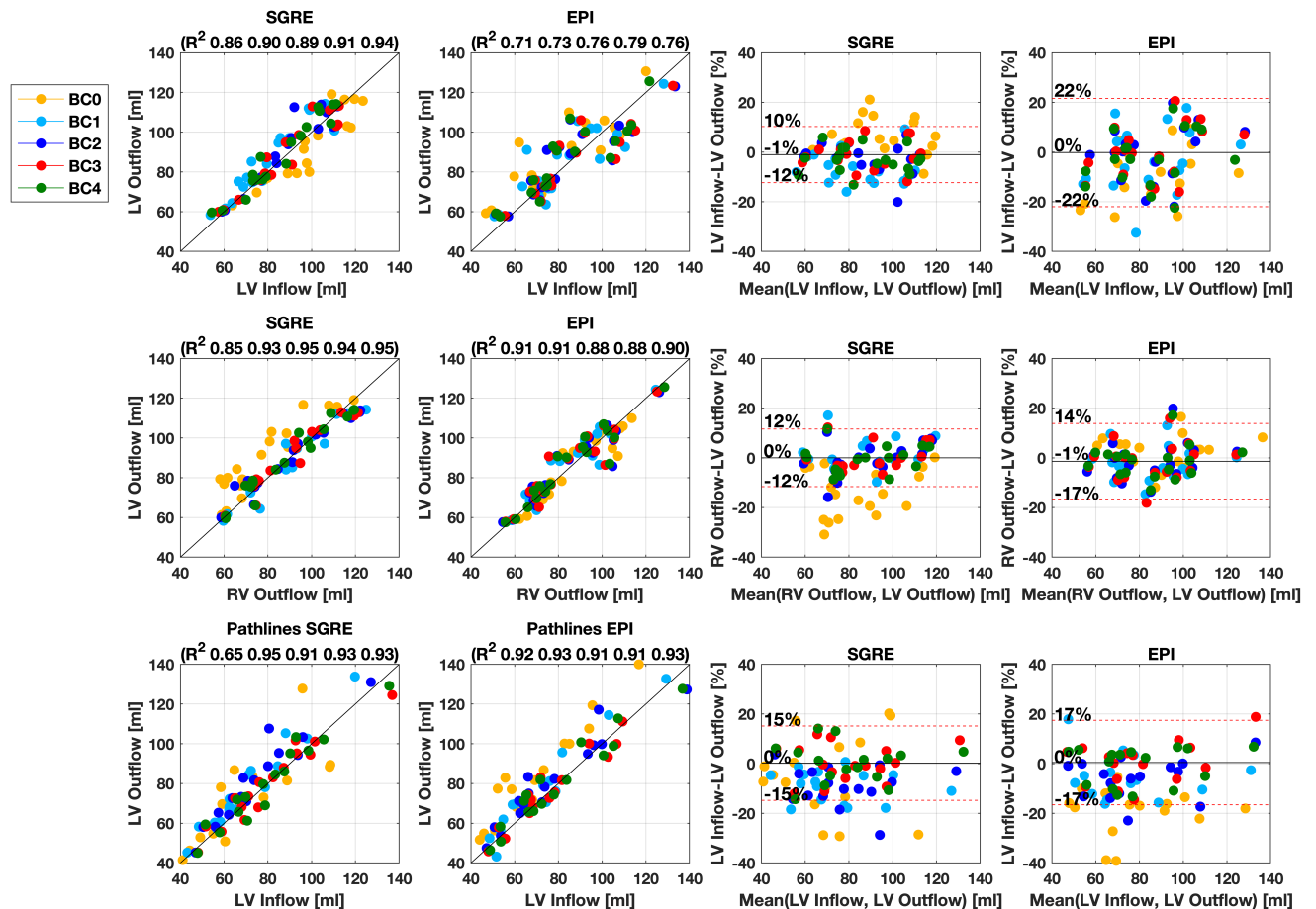


FIGURE 2: Flow volumes obtained for SGRE and EPI measurements, for LV inflow and outflow from transvalvular analysis (a), for LV and RV outflow from transvalvular analysis (b), and LV inflow and outflow from pathline analysis (c). Each color represents a BC order. First and second column: Scatterplots. Third and fourth column: Bland–Altman plots. The black solid line in the scatterplots represents the identity line. The limits of agreements of Bland–Altman plots are relative to BC3 results.

TABLE 2. Volumetric Flow Results (Mean ± SD)

SGRE							
(ml)	LV in	LV out	RV out	Prox DA	Dist DA	In Path	Out Path
BC0	96.3 ± 19.1	90.5 ± 18.8	79.0 ± 19.4	46.0 ± 14.8	52.1 ± 13.2	68.1 ± 22.3	71.2 ± 22.7
BC1	81.2 ± 16.7	87.1 ± 18.4	88.9 ± 20.3	65.8 ± 13.1	58.3 ± 12.6	70.4 ± 19.7	77.2 ± 22.4
BC2	85.9 ± 16.4	88.2 ± 18.1	88.6 ± 21.4	60.5 ± 13.1	57.3 ± 12.0	73.7 ± 20.2	80.8 ± 21.9
BC3	87.7 ± 18.2	88.6 ± 18.0	88.9 ± 21.2	62.5 ± 21.8	57.4 ± 22.3	79.8 ± 22.2	79.5 ± 22.0
BC4	85.9 ± 17.5	88.5 ± 18.5	88.2 ± 19.9	60.8 ± 12.1	57.6 ± 12.0	80.0 ± 22.1	79.9 ± 21.7
EPI							
(ml)	LV in	LV out	RV out	Prox DA	Dist DA	In Path	Out Path
BC0	80.6 ± 20.6	88.3 ± 18.9	90.5 ± 20.9	51.6 ± 9.9	51.6 ± 12.2	69.8 ± 20.4	84.2 ± 24.2
BC1	82.8 ± 20.5	84.4 ± 18.2	82.6 ± 18.3	58.7 ± 12.4	56.9 ± 13.1	73.5 ± 21.8	77.2 ± 23.3
BC2	84.7 ± 21.2	85.2 ± 17.9	84.8 ± 19.5	55.4 ± 12.0	55.0 ± 12.7	76.5 ± 23.7	80.8 ± 22.2
BC3	86.1 ± 21.6	85.5 ± 17.9	84.5 ± 18.7	55.9 ± 11.6	55.0 ± 12.4	80.7 ± 25.4	79.6 ± 20.9
BC4	84.1 ± 20.3	85.8 ± 18.2	84.6 ± 18.9	56.1 ± 11.1	54.8 ± 12.2	79.2 ± 23.7	86.5 ± 22.3

LV in = LV inflow from transvalvular analysis; LV out = LV outflow from transvalvular analysis; RV out = RV outflow from transvalvular analysis; In Path = LV inflow from pathline analysis; Out Path = LV outflow from pathline analysis; Prox DA = proximal descending aorta; Dist DA = distal descending aorta.

are reported in Table 6, as well as the Bland–Altman analysis coefficients. LV outflow EPI measurements were lower than the LVSF at all BC orders. LV outflow SGRE measurements and the LVSF were not statistically different, except for BC1 (*P*-values are reported in Table 6).

Velocity Profile Analysis

The speed at peak systole along a line through a cross-section of the thoracic descending aorta was plotted for both acquisitions (Fig. 1b). The velocity gradients at the wall showed no statistical difference between EPI and SGRE for BC0–4 (*P* = 0.37, 0.36, 0.30, 0.36, 0.52). No difference in peak

velocity was found for BC0–4 between sequences (*P* = 0.61, 0.67, 0.67, 0.76, 0.53). Within each sequence, the BC order had no effect on the profile slope (*P* = 0.12–0.73 SGRE, 0.30–0.72 EPI), nor on the peak velocity (*P* = 0.14–0.17 SGRE, 0.12–0.34 EPI), except for the peak velocity BC0 vs. BC1 (*P* < 0.05 SGRE and EPI), and BC1 vs. BC2 in SGRE.

Discussion

This study investigated and compared the quality of data obtained by respiratory-gated SGRE and EPI 4D Flow MRI sequences and for different background phase offset

TABLE 3. SGRE vs. EPI *P*-Values

	LV in	LV out	RV out	Prox DA	Dist DA	In Path	Out Path	Non-Phys F
BC0	0.00	0.28	0.00	0.04	0.98	0.75	0.00	0.01*
BC1	0.56	0.13	0.00*	0.00*	0.53	0.15	1.00	0.02*
BC2	0.57	0.14	0.04*	0.00*	0.13	0.13	0.98	0.00*
BC3	0.48	0.12	0.03*	0.00*	0.10	0.62	0.95	0.02*
BC4	0.43	0.16	0.03*	0.00*	0.06	0.63	0.89	0.19

The bold formatting indicates *P*-values lower than 0.05 (level of significance).

*SGRE measurements larger than EPIs.

TABLE 4. Paired Student's t-test, Bland-Altman Coefficients, and Linear Regression Model for Valvular Flows

LV inflow vs. outflow SGRE					
	<i>P</i> -values	mean _d [%]	mean _d -2SD	mean _d + 2SD	Linear regression model
BC0	0.00*	6.30	-8.58	21.17	$y = 2.3 + 0.9x$
BC1	0.00	-6.87	-19.37	5.62	$y = 2.4 + 1.0x$
BC2	0.13	-2.26	-14.05	9.53	$y = -1.8 + 1.0x$
BC3	0.51	-1.03	-12.33	10.27	$y = 4.7 + 1.0x$
BC4	0.02	-2.93	-13.31	7.44	$y = 0.5 + 1.0x^2$
	<i>P</i> -values	mean _d [%]	mean _d -2SD	mean _d + 2SD	Linear regression model
BC0	0.01	-10.09	-37.82	17.64	$y = 26.0 + 0.8x$
BC1	0.53	-2.59	-28.45	23.26	$y = 21.7 + 0.8x$
BC2	0.84	-1.37	-24.46	21.72	$y = 23.1 + 0.7x$
BC3	0.81	-0.20	-22.01	21.60	$y = 22.2 + 0.7x$
BC4	0.49	-2.56	-24.54	19.43	$y = 19.8 + 0.8x$
LV vs. RV outflow SGRE					
	<i>P</i> -values	mean _d [%]	mean _d -2SD	mean _d + 2SD	Linear regression model
BC0	0.00	-14.13	-33.35	5.09	$y = 19.8 + 0.9x$
BC1	0.21	1.68	-11.05	14.40	$y = 9.5 + 0.9x$
BC2	0.76	-0.25	-13.13	12.63	$y = 15.0 + 0.8x$
BC3	0.79	-0.01	-11.60	11.59	$y = 11.1 + 0.9x$
BC4	0.79	-0.63	-11.67	10.40	$y = 9.1 + 0.9x$
	<i>P</i> -values	mean _d [%]	mean _d -2SD	mean _d + 2SD	Linear regression model
BC0	0.17	2.22	-11.47	15.90	$y = 10.3 + 0.9x$
BC1	0.19	-2.28	-15.73	11.17	$y = 6.4 + 0.9x$
BC2	0.79	-0.91	-16.02	14.20	$y = 12.3 + 0.9x$
BC3	0.52	-1.40	-16.62	13.83	$y = 9.9 + 0.9x$
BC4	0.43	-1.51	-14.77	11.74	$y = 8.4 + 0.9x$
Pathline analysis inflow vs. outflow SGRE					
	<i>P</i> -values	mean _d [%]	mean _d -2SD	mean _d + 2SD	Linear regression model
BC0	0.39	-4.63	-37.38	28.12	$y = 15.4 + 0.8x$
BC1	0.00	-8.95	-21.68	3.78	$y = -1.1 + 1.1x$
BC2	0.00	-8.96	-24.72	6.81	$y = 4.5 + 1.0x$
BC3	0.84	0.19	-14.78	15.15	$y = 7.6 + 0.9x$
BC4	0.92	0.20	-15.52	15.91	$y = 4.1 + 0.9x$
	<i>P</i> -values	mean _d [%]	mean _d -2SD	mean _d + 2SD	Linear regression model
BC0	0.00	-18.71	-37.47	0.05	$y = 4.6 + 1.1x$
BC1	0.02	-4.69	-22.56	13.18	$y = 1.2 + 1.0x$
BC2	0.03	-6.07	-22.30	10.16	$y = 12.6 + 0.9x$

TABLE 4. Continued

LV inflow vs. outflow SGRE					
	<i>P</i> -values	mean _d [%]	mean _d -2SD	mean _d + 2SD	Linear regression model
BC3	0.60	0.44	-16.57	17.46	$y = 16.2 + 0.8x$
BC4	0.74	-0.97	-16.28	14.35	$y = 7.9 + 0.9x$

The bold formatting indicates *P*-values lower than 0.05 (level of significance), and mean_d lower than 5%.
 *Inflow larger than outflow. All linear regression models were statistically significant.

corrections. In general, both acquisitions showed good internal data consistency for transvalvular flow volumes when appropriate background phase offset correction was applied. LV stroke volumes assessed from EPI-based 4D Flow MRI data showed to be lower than short-axis-based stroke volumes. EPI 4D flow MRI volumetric flows at the pulmonary valve and at the proximal descending aorta were also lower compared with SGRE.

The BC order had minor effects on the determination coefficients of LV flows and LV outflow vs. RV outflow, for both sequences, excluding BC0. This is not surprising, as the cardiac valves are located closely and are therefore similarly affected by background phase offset. The Bland–Altman plots for transvalvular flow analysis showed that the mean_d of the compared quantities, eg, inflow vs. outflow, became lower than 5% with BC2-to-4 in SGRE and BC1-to-4 in EPI. A limit of acceptability of 5% error in stroke volume was considered acceptable by Gatehouse et al.³¹ Similarly, pathline analysis yielded better results for BC3-to-4 in both sequences, as the mean_d was lower than 5%, and the nonphysiological

flow at its minimum, which was 18% and 17% for SGRE and EPI, respectively. The EPI nonphysiological flow at any BC order except 4 was lower compared with SGRE. Altogether, EPI data were less sensitive to BC order variation, and a first-order BC was sufficient for transvalvular analysis, while for SGRE data at least a second-order BC was necessary. However, EPI data quality does not seem to be decreased, but potentially increased, at higher than first BC order. Third and fourth BC order are preferred for pathline analysis.

The results obtained using transvalvular and pathline analysis differ up to the 5–10%. The two techniques evaluate different data quality aspects: While the transvalvular analysis is based on assessing flow directly on the flow images, pathline analysis, due to the integration over time, is more sensitive to artifacts like background offset and noise, and noise-related errors do not cancel out, but rather result in a decreased volume flow. As for the pathline analysis, the proportion of nonphysiological compared with physiological flow gives an indication of the data quality, as the same segmentation was used for the analysis of SGRE and EPI.

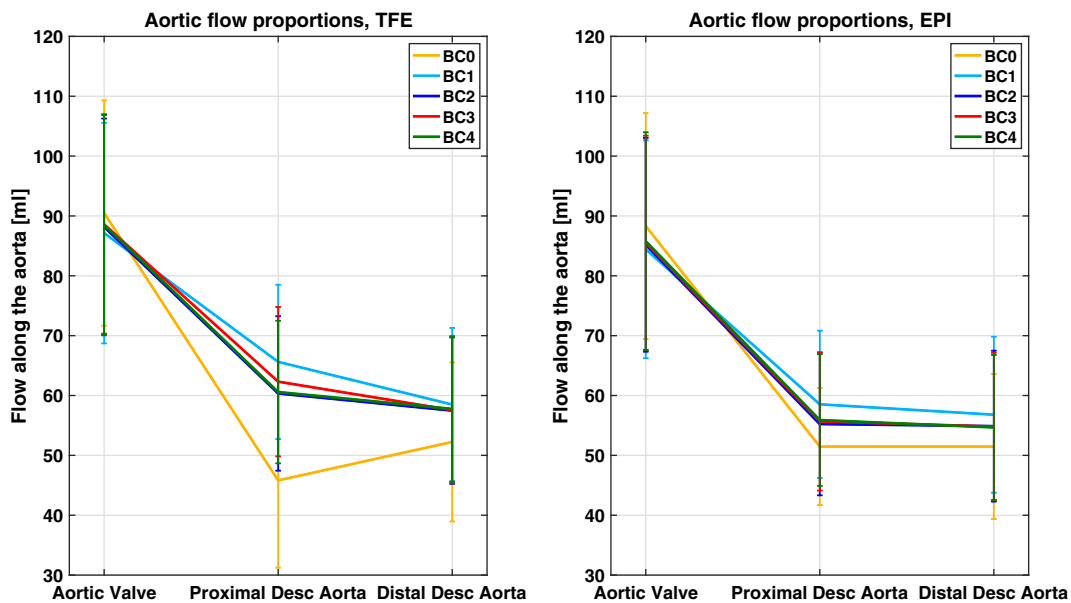


FIGURE 3: Volumetric flow results along the aorta for SGRE and EPI measurements. All the flows are reported as mean of all volunteers and standard deviation.

TABLE 5. Nonphysiological Flow

	Nonphysiological flow				
	Mean \pm SD		<i>P</i> -values		
	SGRE [%]	EPI [%]		SGRE	EPI
BC0	38.5 \pm 16.0	24.5 \pm 5.8	—	—	—
BC1	26.8 \pm 6.1	21.8 \pm 7.4	Δ BC(0–1)	0.01	0.07
BC2	23.8 \pm 5.0	18.7 \pm 4.3	Δ BC(1–2)	0.01	0.04
BC3	18.9 \pm 4.3	16.7 \pm 4.0	Δ BC(2–3)	0.00	0.00
BC4	18.0 \pm 4.3	17.0 \pm 4.2	Δ BC(3–4)	0.05	0.19

The bold formatting indicates *P*-values lower than 0.05 (level of significance).

Outflow and inflow LV volumes depend on this proportion too, becoming more accurate as nonphysiological flow diminishes, hence as the BC order increases.

The optimal polynomial order for the background correction should depend on the amount of static tissue present in the data, used to compute the polynomial fit. The amount of static tissue present in the datasets used in this study was around 40–45% of the total acquired volume, hence less than the minimum recommended by Busch et al, ie, 60%, for second-order correction, and 75% for higher orders.²⁴ Our data indicate an improvement of data quality for increasing background correction orders. We believe that a soft mask, as used here, requires less static tissue than a conventional hard

threshold mask, thus allowing higher-order polynomial fits for the background correction. In order to assess the effect of different order polynomial correction, a common approach is to perform measurements on a static phantom, instead of the in vivo experiments. However, as the in vivo measurements would inherently differ from the in vitro, due to, eg, eddy currents and respiratory effects, any conclusion concerning the background correction derived from static phantom experiments would not represent any useful "ground truth." Hence, in this study we have not done any phantom experiment. Furthermore, since different MR systems may create different background phase offset patterns, different approaches and tunings may be required for the correction,³¹ so every

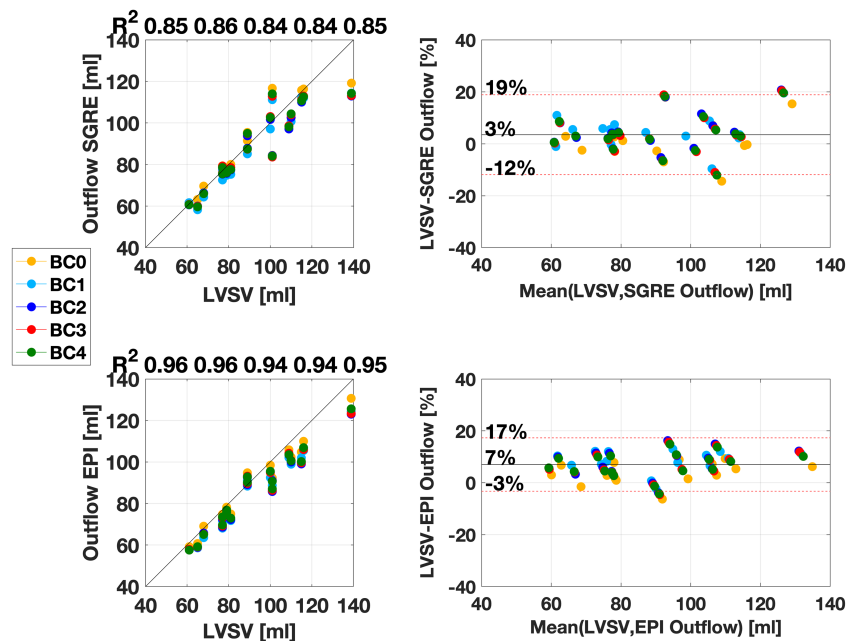


FIGURE 4: LVSV and LV outflow obtained for SGRE and EPI measurements from transvalvular analysis. Each color represents a BC order. First column: Scatterplots. Second column: Bland–Altman plots. The black solid line in the scatterplots represents the identity line. The limits of agreements of Bland–Altman plots are relative to BC3 results.

TABLE 6. Paired Student’s t-test, Bland-Altman Coefficients, and Linear Regression Model Between the LVSV and SGRE- EPI LV Outflow

LVSV vs. SGRE LV outflow					
	<i>P</i> -values	mean _d [%]	mean _d -2SD	mean _d + 2SD	Linear regression model
BC0	0.45	1.35	-14.10	16.80	$y = 13.9 + 0.8x$
BC1	0.02*	5.21	-9.37	19.79	$y = 11.4 + 0.8x$
BC2	0.07	3.92	-11.35	19.20	$y = 14.7 + 0.8x$
BC3	0.10	3.47	-11.89	18.83	$y = 14.5 + 0.8x$
BC4	0.09	3.57	-11.62	18.76	$y = 13.4 + 0.8x$
LVSV vs. EPI LV outflow					
	<i>P</i> -values	mean _d [%]	mean _d -2SD	mean _d + 2SD	Linear regression model
BC0	0.00*	3.87	-5.57	13.31	$y = 6.7 + 0.9x$
BC1	0.00*	8.39	-0.44	17.23	$y = 5.5 + 0.8x$
BC2	0.00*	7.41	-2.94	17.77	$y = 8.4 + 0.8x$
BC3	0.00*	7.02	-3.24	17.29	$Y = 8.5 + 0.8x$
BC4	0.00*	6.78	-3.02	16.58	$y = 7.2 + 0.8x$

The bold formatting indicates *P*-values lower than 0.05 (level of significance).
 *LVSV larger than the compared quantity. All linear regression models were statistically significant.

solution regarding the optimal background correction strategy could be confined to specific systems and conditions.

When BC was applied, the flow measurements were lower for EPI than for SGRE data, at the pulmonary valve and at the proximal descending aorta. The comparison with LVSV showed that EPI LV outflows were lower at all BC orders, while no significant difference was found between LVSV and SGRE with BC2-4. This indicates that the EPI measurements were underestimated, rather than the SGRE overestimated. This underestimation of EPI flow might be due to smoothing as a result of field inhomogeneities³² and the large and variable time difference between the velocity measurement and spatial encoding. To test this effect in our data, we checked the velocity profile at peak systole over a center line at the cross-section of descending thoracic aorta. The difference in slope of the SGRE and EPI curve was not significant, but there is a trend towards lower velocity gradients at the wall and smaller peak velocity for EPI than for SGRE. This might explain the lower volume seen in the EPI flow measurements. In addition to the smoothing effect of EPI, the difference to SGRE could be also due to remaining background offsets. The proximal descending aortic plane was located in the highest part of the acquisition volume, ie, farthest from the magnet isocenter, where eddy current effects are more severe. As for the RV outflow, the SGRE and EPI means differ by 10% at BC0-1 and by 5% at BC2-4. EPI

RV outflow changed significantly when stepping from BC0 to BC1 and again from BC1 to BC2, while did not change in SGRE except when increasing BC0 to BC1, indicating that those residual phase errors were mostly in the EPI measurements.

According to the Wilcoxon test for the visual inspection of the phase and magnitude images (*P* = 0.08), there was no difference between the sequences. The *P*-value is, however, close to significance, suggesting a possible trend toward a difference, which can be explained by the appearances of the phase and especially the magnitude images, slightly different between SGRE and EPI. The smoothing effect in EPI can in fact give the impression of reduced noise levels and respiration artifacts, which can be judged positive or negative. Nevertheless, the results obtained with the two validation techniques proved that both sequences can produce good results (strong and very strong association, mean_d < 5%), when BC is applied. Despite the strong association values, the EPI measurements in our experiments presented a larger spread compared with SGRE, particularly visible in the Bland–Altman plots of LV inflow vs. outflow.

A recent study by Garg et al compared SGRE with *k*-space segmentation factor 2 and EPI with read-out factor 5 and concluded that EPI was superior to SGRE.¹⁹ This is in conflict with our findings. Interestingly, we obtained similar results as Garg et al for EPI ($y = 0.73x + 22.23$, $R^2 = 0.79$

vs. $y = 0.89x + 12.08$, $R^2 = 0.87$, with $x = \text{LV inflow}$ and $y = \text{LV outflow}$), but considerably better results for SGRE when compared with the results in Garg et al ($y = 0.96x + 4.74$, $R^2 = 0.91$ vs. $y = 0.74x + 27.00$, $R^2 = 0.34$). Garg et al speculate that the better EPI performance found in their study could be explained by a shorter acquisition time that could have reduced respiratory artifacts in their non-respiratory motion suppressed sequences. Here, we employed a respiratory navigator, as it drastically decreases errors associated with respiratory motion in 4D Flow MRI.³³ Indeed, the results for SGRE were considerably better in our study, but we find it unlikely that the lack of respiratory motion compression would affect the SGRE and EPI sequence very differently. In both studies, the difference in scan time between the EPI and SGRE sequence was less than 10%, which seems too small to cause such a large reduction in data quality. However, Garg et al¹⁹ also found a large number of SGRE datasets containing severe artifacts, which we did not find in our study and have not seen in our studies without respiratory motion suppression either.²⁶ Therefore, we speculate that the SGRE sequence used by Garg et al, despite having similar scan parameters, was differently tuned when compared with our sequence.

This study has several limitations. Only healthy volunteers were studied and, due to its long readouts, EPI-based 4D Flow can be suspected to perform worse in patients with valvular stenosis or regurgitation and associated turbulent flow.^{34,35} Another limitation is that only EPI factor 3 was fully evaluated in this study. By increasing the read-out factor, shorter scan times can be achieved at the cost of a potential reduction in data quality.

In conclusion, this study shows that both SGRE and EPI 4D Flow MRI result in good internal data consistency in healthy volunteers when an adequate background correction is applied. Second-order background correction, to reduce the eddy-current-induced phase offsets, results in good internal data consistency for SGRE for transvalvular flow analysis. A first-order correction may be sufficient for EPI. Third and fourth BC orders are preferred when performing particle trace analysis in both sequences. EPI 4D Flow MRI may underestimate volumetric flow compared with short-axis based stroke volume assessment and SGRE 4D Flow MRI.

Acknowledgment

The authors thank Hojin Ha, PhD, for his contribution in the image quality evaluation.

References

1. Hope MD, Meadows AK, Hope TA, et al. Clinical evaluation of aortic coarctation with 4D flow MR imaging. *J Magn Reson Imaging* 2010;31:711–718.
2. Nordmeyer S, Riesenkampff E, Messroghli D, et al. Four-dimensional velocity-encoded magnetic resonance imaging improves blood flow quantification in patients with complex accelerated flow. *J Magn Reson Imaging* 2013;37.
3. Valverde I, Nordmeyer S, Uribe S, et al. Systemic-to-pulmonary collateral flow in patients with palliated univentricular heart physiology: Measurement using cardiovascular magnetic resonance 4D velocity acquisition. *J Cardiovasc Magn Reson* 2012;14:25.
4. Hanneman K, Sivagnanam M, Nguyen ET, et al. Magnetic resonance assessment of pulmonary (Q P) to systemic (Q S) imaging. *Acad Radiol* 2014;21:1002–1008.
5. Roes SD, Hammer S, van der Geest RJ, et al. Flow assessment through four heart valves simultaneously using 3-dimensional 3-directional velocity-encoded magnetic resonance imaging with retrospective valve tracking in healthy volunteers and patients with valvular regurgitation. *Invest Radiol* 2009;44:669–675.
6. Dyverfeldt P, Bissell M, Barker AJ, et al. 4D flow cardiovascular magnetic resonance consensus statement. *J Cardiovasc Magn Reson* 2015;17:72.
7. Pruessmann KP, Weiger M, Scheidegger MB, Boesiger P. SENSE: Sensitivity encoding for fast MRI. *Magn Reson Med* 1999;42:952–962.
8. Griswold MA, Jakob PM, Heidemann RM, et al. Generalized autocalibrating partially parallel acquisitions (GRAPPA). *Magn Reson Med* 2002;47:1202–1210.
9. Tsao J, Boesiger P, Pruessmann KP. k-t BLAST and k-t SENSE: Dynamic MRI with high frame rate exploiting spatiotemporal correlations. *Magn Reson Med* 2003;50:1031–1042.
10. Balthes C, Kozerke S, Hansen MS, Pruessmann KP, Tsao J, Boesiger P. Accelerating cine phase-contrast flow measurements using k-t BLAST and k-t SENSE. *Magn Reson Med* 2005;54:1430–1438.
11. Davis CP, McKinnon GC, Debatin JF, et al. Normal heart: Evaluation with echo-planar MR imaging. *Radiology* 1994;191:691–6.
12. Debatin rg F, Davis CP, Felblinger J, McKinnon GC. Evaluation of ultrafast phase-contrast imaging in the thoracic aorta. *MAGMA* 1995;3:59–66.
13. Petersson S, Sigfridsson A, Dyverfeldt P, Carlhäll C-J, Ebbers T. Retrospectively gated intracardiac 4D flow MRI using spiral trajectories. *Magn Reson Med* 2016;75:196–206.
14. Ma LE, Markl M, Chow K, et al. Aortic 4D flow MRI in 2 minutes using compressed sensing, respiratory controlled adaptive k-space reordering, and inline reconstruction. *Magn Reson Med* 2019;81:3675–3690.
15. Bollache E, Barker AJ, Dolan RS, et al. k-t accelerated aortic 4D flow MRI in under two minutes: Feasibility and impact of resolution, k-space sampling patterns, and respiratory navigator gating on hemodynamic measurements. *Magn Reson Med* 2018;79:195–207.
16. Santelli C, Loecher M, Busch J, Wieben O, Schaeffter T, Kozerke S. Accelerating 4D flow MRI by exploiting vector field divergence regularization. *Magn Reson Med* 2016;75:115–125.
17. Westenberg JJM, Roes SD, Ajmone Marsan N, et al. Mitral valve and tricuspid valve blood flow: Accurate quantification with 3D velocity-encoded MR imaging with retrospective valve tracking. *Radiology* 2008;249:792–800.
18. van der Hulst AE, Westenberg JJM, Kroft LJM, et al. Tetralogy of Fallot: 3D Velocity-encoded MR imaging for evaluation of right ventricular valve flow and diastolic function in patients after correction. *Radiology* 2010;256:724–734.
19. Garg P, Westenberg JJM, van den Boogaard PJ, et al. Comparison of fast acquisition strategies in whole-heart four-dimensional flow cardiac MR: Two-center, 1.5 Tesla, phantom and in vivo validation study. *J Magn Reson Imaging* 2017;47:272–281.
20. Caprihan A, Altobelliand SA, Benitez-Read E. Flow-velocity imaging from linear regression of phase images with techniques for reducing eddy-current effects. *J Magn Reson* 1990;90:71–89.

21. Walker PG, Cranney GB, Scheidegger MB, Waseleski G, Pohost GM, Yoganathan AP. Semiautomated method for noise reduction and background phase error correction in MR phase velocity data. *J Magn Reson Imaging* 1993;3:521–30.
22. Lankhaar J-W, Hofman MBM, Marcus JT, Zwanenburg JJM, Faes TJC, Vonk-Noordegraaf A. Correction of phase offset errors in main pulmonary artery flow quantification. *J Magn Reson Imaging* 2005;22:73–79.
23. Chernobelsky A, Shubayev O, Comeau CR, Wolff SD. Baseline correction of phase contrast images improves quantification of blood flow in the great vessels. *J Cardiovasc Magn Reson* 2007;9:681–685.
24. Busch J, Giese D, Kozerke S. Image-based background phase error correction in 4D flow MRI revisited. *J Magn Reson Imaging* 2017;46:1516–1525.
25. Ebbers T, Haraldsson H, Dyverfeldt P. Higher order weighted least-squares phase offset correction for improved accuracy in phase-contrast MRI. In: *Proc 16th Annual Meeting ISMRM, Toronto; 2008*. p 1367.
26. Wigström L, Ebbers T, Fyrenius A, et al. Particle trace visualization of intracardiac flow using time-resolved 3D phase contrast MRI. *Magn Reson Med* 1999;41:793–799.
27. Westenberg JJM, Doornbos J, Versteegh MIM, et al. Accurate quantitation of regurgitant volume with MRI in patients selected for mitral valve repair. *Eur J Cardio Thoracic Surg* 2005;27:462–467.
28. Lucas BD. An iterative image registration technique with an application to stereo vision. In: *Proc IJCAI'81 Proc 7th Int Jt Conf Artif Intell* 1981;130.
29. Eriksson J, Carlhäll CJ, Dyverfeldt P, Engvall J, Bolger AF, Ebbers T. Semi-automatic quantification of 4D left ventricular blood flow. *J Cardiovasc Magn Reson* 2010;12:9.
30. Heiberg E, Sjögren J, Ugander M, Carlsson M, Engblom H, Arheden H. Design and validation of Segment—Freely available software for cardiovascular image analysis. *BMC Med Imaging* 2010;10:1.
31. Gatehouse PD, Rolf MP, Graves MJ, et al. Flow measurement by cardiovascular magnetic resonance: A multi-centre multi-vendor study of background phase offset errors that can compromise the accuracy of derived regurgitant or shunt flow measurements. *J Cardiovasc Magn Reson* 2010;12:5.
32. Debatin JF, Leung DA, Wildermuth S, Botnar R, Felblinger J, McKinnon GC. Flow quantitation with echo-planar phase-contrast velocity mapping: In vitro and in vivo evaluation. *J Magn Reson Imaging* 1995;5:656–662.
33. Dyverfeldt P, Ebbers T. Comparison of respiratory motion suppression techniques for 4D flow MRI. *Magn Reson Med* 2017;78:1877–1882.
34. Ståhlberg F, Thomsen C, Söndergaard L, Henriksen O. Pulse sequence design for MR velocity mapping of complex flow: Notes on the necessity of low echo times. *Magn Reson Imaging* 1994;12:1255–1262.
35. O'Brien KR, Cowan BR, Jain M, Stewart RAH, Kerr AJ, Young AA. MRI phase contrast velocity and flow errors in turbulent stenotic jets. *J Magn Reson Imaging* 2008;28:210–218.